Comparison of the Effects of Tissue Processing on the Physicochemical Properties of Bone Allografts

Elnaz Ajami, MSc, PhD[1]/Cong Fu, MEng, PhD[1]/Sun Jin Park, MSc, PhD[1]/
Xuesong Wang, MSc, PhD[1]/Hai Bo Wen, MSc, PhD[1]

Purpose: To address the hypothesis that the tissue processing methods of solvent dehydration and freeze-drying would differentially affect the physicochemical characteristics of four commercially available bone allografts and the adhesion and differentiation of human bone marrow–derived mesenchymal stromal cells (hBMSCs) on such substrates in vitro. ***Materials and Methods:*** The surface morphology, surface area, and elemental composition of four commercially available cancellous bone allografts were examined using SEM, Brunauer-Emmett-Teller (BET) gas adsorption, and inductively coupled plasma (ICP) analyses. SEM was also employed to compare the allograft surfaces to that of human bone exposed by in vitro osteoclastic resorption. The allografts were seeded with hBMSCs, and the number of adhered cells was assessed at 3 and 7 days. Alkaline phosphatase (ALP) activity was quantified as a measure of osteogenic differentiation after 21 days. ***Results:*** Marked differences were seen between the physicochemical characteristics of the solvent-dehydrated and freeze-dried allografts, as well as between their resulting bone microarchitectures and that of osteoclast-resorbed human bone. Increased hBMSC adhesion and differentiation were observed on the solvent-dehydrated allografts compared to freeze-dried allografts, which suggests a higher putative osteogenic potential. The latter was attributed to better preservation of the bone collagen microarchitecture integrity, which may provide not only a more complex substrate architecture, but also a more favorable microenvironment to allow nutrients and oxygen to flow to the adhered cells. ***Conclusion:*** Commercially available cancellous bone allografts significantly differ in their physicochemical characteristics, stemming from differences in tissue processing and sterilization methods undertaken by tissue banks. These differences impact the response of MSCs in vitro and may alter the biologic performance of the grafts in vivo. Therefore, it is important to consider these characteristics when choosing a bone substitute for clinical application, as the physicochemical properties of the grafts play a crucial role in their interactions with the biologic environment and subsequent incorporation into the native bone. *Int J Oral Maxillofac Implants 2023;38:169–180. doi: 10.11607/jomi.9781*

Oral implantology has evolved over the past few decades, and patient quality of life has significantly improved through the use of dental implant rehabilitation.[1] Bone reconstruction procedures that use bone grafts are often required for optimal implant placement positioning. Depending on the extent of atrophy in the alveolar crest, bone grafts may be performed either in conjunction with the implant placement or as a separate procedure.[2] The net biologic activity of a bone graft is determined by the combination of its inherent biologic activity (ie, living cells), its capacity to activate surrounding host tissues to relevant biologic activity (ie, osteoinduction mediated by bioactive factors within the matrix), and its ability to support the ingrowth of osteogenic host tissue (ie, osteoconduction).[3]

Autogenous bone grafting has long been regarded as the gold standard for bone reconstruction and is currently the only form of bone grafting that possesses osteoconductive, osteoinductive, and osteogenic properties.[2,4] It offers the advantage of rapid and complete incorporation into the host bone site with an absence of immunologic reactions. The incorporation of cancellous bone autografts is a well-established phenomenon, characterized by the formation of new bone over the graft bed through the dual remodeling processes of resorption and bone formation. Following graft placement, a local hematoma forms, leading to an inflammatory response and the recruitment of neutrophils, macrophages, and endothelial cells into the graft. The released cytokines and growth factors lead to the recruitment of host perivascular mesenchymal stromal progenitor cells (MSCs), which comprise the granulation tissue and extracellular matrix. Indeed, the removal of the graft material starts slowly, in conjunction with the occurrence of neovascularization. Finally, the bone graft is incorporated into de novo bone. Osteoblasts line the periphery of the graft and produce osteoid, which is then mineralized to form new bone. A successful outcome depends on the appropriate balance

[1]Zimmer Biomet Dental, Palm Beach Gardens, Florida, USA.

Correspondence to: Dr Elnaz Ajami, Research and Development, Zimmer Biomet Dental, 4555 Riverside Drive, Palm Beach Gardens, FL, 33410, USA; Email: elnaz.ajami@zimmerbiomet.com

Submitted November 23, 2021; accepted June 17, 2022.

between the biologic activity of the bone graft, the condition of the perigraft environment, and the mechanical environment.[3]

Due to several difficulties associated with autografts, such as an increased risk of infection, additional surgical sites, harvesting morbidity, and restricted bone supply,[5] allografts or xenografts are chosen as pragmatic alternatives. Cancellous allograft incorporation differs from autograft incorporation in several ways. While cancellous allografts tend to be characterized by a progressive creeping substitution by means of vascular channels and resorbed cavities covered by a layer of new bone, both vascular penetration and bone formation occur at a slower pace and to a less extensive degree than in autografts. This is considered to be due, in part, to the tissue processing and sterilization techniques employed following the retrieval of the bone tissue from its cadaveric source, which is necessary to reduce both the risk of infection and induction of immunologic reaction in the grafted recipient.[6]

Thus, successful biological outcomes using allografts and xenografts depend on their level of sterility and the thorough removal of immunogenic materials via freezing or blood and cellular constituent removal. This is usually achieved using a combination of chemicals (Triton X-100, sodium dodecyl sulfate, hydrogen peroxide), enzymes (DNAse, trypsin), and physical treatment (centrifugation, sonication, temperature treatment).[7] The donated tissue for the allografts goes through three steps of donor screening, tissue processing and packaging, and terminal sterilization before it is delivered for implantation. After the donor screening process, several steps are taken to ensure standardized tissue processing with aseptic techniques, which incorporate standard operating room techniques. Sterilization is then followed to achieve the AATB-established Sterility Assurance Level (SAL) 10.[6,8]

Most tissue banks use tissue processing via freeze-drying (lyophilization), which allows the allograft tissue to be stored at room temperature in a sealed package. This lyophilization process freezes the tissue at about –80°C for 1 to 2 weeks, and the water content is reduced to less than 6% of its initial weight.[8] This reduction of water content does not support any biologic activity or chemical reactions in the tissue. A different dehydration approach to lyophilization is based on the use of solvents.[9]

Different terminal sterilization techniques are employed by the tissue banks across the United States to achieve an SAL of 10^{-6}. While some tissue banks apply gamma irradiation with varying radiation doses from one tissue bank to another, others may use electron beam technology. While the latter uses machine-generated high-energy electrons, the former is comprised of photons generated by the decay of a radioactive nucleus (eg, cobalt-60). As electrons have mass, the penetration is limited by the amount of energy; however, though photons have no mass and may penetrate deeper into matter, no changes can be made to affect their energy spectrum.[10]

It is fundamental to ensure that the applied allograft processing methods can effectively inactivate viruses, kill bacteria, penetrate into the tissue, and be safely removed while preserving the biomechanical and biologic properties of the tissue.[8] However, during tissue processing, it is not possible to entirely prevent changes that occur in the physicochemical properties of the graft, such as surface area, surface structure, chemical composition, and mechanical stability. Such changes may, in turn, influence the biologic performance of the graft. While the role of the surface chemistry and the ionic exchange between the surface of a biomaterial implanted in a bone defect with the biologic fluid cannot be neglected, surface physical characteristics play a more crucial role in the phenomenon of osteoconduction and the subsequent osseointegration process. Surfaces with higher degrees of complexity favor the stabilization of blood clots and subsequent platelet adhesion and activation.[11] Platelet releasate provides signaling cytokines to recruit perivascular progenitors to migrate from their niche towards the graft surface, differentiate down the osteogenic lineage, and initiate new bone formation on the surface.[12] Therefore, when processing allografts, it is crucial to ensure that the native bone microarchitecture is preserved to the best possible extent and is not damaged or considerably altered in terms of surface characteristics in order to ensure a strong interface between the newly formed bone and allograft particulates.

The present authors hypothesize that the differences in the processing and sterilization of the donor tissue differentially affect the physicochemical characteristics of the final product, and thus potentially affect the MSC response. While some studies have investigated the physicochemical characteristics of commercial bone grafts, they have included a variety of bone xenografts, allografts, and synthetic materials.[13–15] In the reviewed published literature, there was no direct comparison between commercial allografts as a function of their processing methods. Therefore, this study investigated the impact of different processing methods on the physicochemical properties of four commercially available cancellous allografts used in implant dentistry. The impact of such physicochemical differences on the adherence and osteogenic differentiation of human mesenchymal progenitors were also examined in vitro.

MATERIALS AND METHODS

Allografts

Four different commercially available mineralized cancellous bone allografts were investigated (Table 1). All

Table 1 List of the Bone Allografts and Related Processing and Sterilization Methods

Allograft	Manufacturer	Distributor	Graft information	Cleaning and preservation	Sterilization
Puros (PTA)	RTI Biologics	Zimmer Biomet	Mineralized, cancellous, 0.25–1 mm	Solvent dehydration (Tutoplast)	Gamma
Creos (CFA)	Community Tissue Services	Nobel Biocare	Mineralized, cancellous, 0.25–1 mm	Freeze-dried	Gamma
OraGraft (OFA)	LifeNet Health	LifeNet Health	Mineralized, cancellous, 0.25–1 mm	Freeze-dried	Gamma
MinerOss (MFA)	Precision Allograft Solutions	Alamo Tissue Service exclusively for BioHorizons	Mineralized, cancellous, 0.3–1 mm	Freeze-dried	Electron beam

of the allografts were obtained directly from their manufacturers in sealed vials of their lowest available particle size range and evaluated without alteration.

Puros allograft (PTA; Zimmer Biomet) is treated with the proprietary Tutoplast process (RTI Biologics). The process involves delipidization using acetone and an ultrasound, osmotic treatment using distilled water and a saline bath, oxidative treatment using a hydrogen peroxide solution, and serial dehydration. After processing, the result is a nondemineralized allograft containing all of the minerals and the collagen matrix structure of the native bone tissue.[9] Low-dose gamma irradiation is applied terminally to the product to achieve an SAL of 10^{-6}.[8,16]

Creos allograft (CFA; Nobel Biocare) is a freeze-dried allograft obtained from Community Tissue Services and processed via a proprietary method and gamma-irradiated to an SAL of 10^{-6}.

OraGraft allograft (OFA; LifeNet Health) is processed via patented Allowash XG freeze-drying technology, which incorporates a scrubbing technique and intensive decontamination steps with alcohol, antibiotics, and hydrogen peroxide with ultrasonication, followed by centrifugation and/or microabsorption to remove excess water and any remaining processing residuals.[8,16] A terminal low-dose gamma sterilization step is applied to inactivate viruses and render an SAL of 10^{-6} without adversely affecting the biomechanical or biochemical properties of the tissue for the intended clinical application.[17]

MinerOss allograft (MFA; BioHorizons) is processed via a freeze-drying method. The tissue is obtained from Precision Allograft Solutions, which is irradiated via electron beam methodology with a target range of 15 to 25 kGy to allow for low-dose irradiation to achieve an SAL level of 10^{-6}.

In addition, the allograft surfaces were able to be compared to the osteoclast-resorbed surface of human bone through the generous gift of samples provided by the University of Toronto for a previously published study, as described by Ay et al.[18] These samples were carbon sputter-coated and used as-received to examine the surface morphology using a field-emission SEM (FESEM; JSM-IT500 HR, JEOL) under the same working conditions described below.

Physical and Chemical Characterization of the Allografts

For each of the characterization experiments, a total of three vials of each sample type from different lots were used. If the bone graft from one vial was used for multiple analyses, the vial with the remaining bone graft was sealed and kept in an ambient environment until used.

Surface Morphology

The surface morphology of the allografts were characterized using FESEM. The bone graft vials of three different lots were opened, and the particulates were poured onto a conductive carbon tape mounted on a sample holder. The holder was then tapped a few times to remove any loosely bound particulates prior to sputter-coating with gold for imaging. Images were taken of the surface morphology at a series of magnifications in back-scattered mode and an accelerating voltage of 5 to 10 kV to examine the microarchitecture of the bone tissue.

Surface Roughness

The surface roughness (Sa; the arithmetic average of the peaks and valleys of a surface in profile) of the allografts were measured from the SEM images taken at × 10,000 magnification using MountainsMap SEM Topo 7.4 surface imaging and analysis software (Digital Surf). The SEM images were reconstructed to convert the luminance information to topography, considering a 100-µm height range. The Sa was then assessed from the reconstructed image using a Gaussian filter with a 2.5-µm cutoff to filter out the surface ends and remove waviness.

Specific Surface Area

The Brunauer-Emmett-Teller (BET) gas adsorption surface area analysis based on krypton absorption (AutoFlow BET+, Quantachrome Instruments) was applied to measure the specific surface area of the allografts. Three

vials from three different lots (n = 3 per sample type) of each sample type were opened, and a minimum of 2 g of each sample was weighted directly from the as-received vials. The size and the number of particles in the 2 g of material was not quantified. The material was then outgassed at 25°C for 16 hours and then placed in the test station. A multipoint krypton adsorption program (n ≥ 6) was used to obtain an adsorption isotherm and calculate the specific surface area, with the material measured in m^2/g. Three samples from each group were tested.

Microhardness

To measure the microhardness values of the allografts, the particulates were first mounted in phenolic resin. The surface was then polished with 400- to 2,000-grit sandpapers under constant irrigation, then stained with acrylic paint (Craft Smart) in order to better distinguish the bone particulates from surrounding resin material. The Vickers hardness was evaluated using a microhardness tester (1600 series, Buehler) under 50 gf. Five locations from each group were tested. The tests were repeated three times with samples from three different lots.

Phase Constitution

The crystallographic structures of the allografts were determined via x-ray diffraction (XRD; X'Pert Pro diffractometer, PANalytical) with CuKα radiation (λ = 1.5418 Å) at 45 KV/40 mA. Diffraction scans were run in the range of 5 to 90 degrees, with a step size of 0.0131 degrees and a counting time of 250 seconds per step. The crystalline phase was identified with the aid of the Powder Diffraction File published by the International Centre for Diffraction Data or the Inorganic Crystal Structure Database (ICSD). The crystallite size was calculated using the Scherrer equation:

$$\tau = \frac{0.9\lambda}{B \cdot \text{Cos}\theta}$$

where λ represents the wavelength of CuKα (ie, 0.154 nm), B is the full width at the half-maximum intensity of the hydroxyapatite (HA) peak (211) of plane in radians, and θ is the angle of this peak in degrees (Bragg diffraction angle). Three samples from three different lots from each group were tested, and an average crystallite size was calculated.

Elemental Analysis

Elemental analysis was conducted based on CAP-017 N (ICP-AES), ASTM 1019-11 (Comb./IGF), and ASTM E1409-13 (IGF). Weight percentages of calcium, phosphorous, and nitrogen were accurately measured. Three samples of three different lots from each group were tested.

Human Bone Marrow–Derived Mesenchymal Stem Cell Cultures

Cell adhesion on the allografts. Allografts were removed from their original packaging under sterile conditions, and 85 ± 0.8 mg of each allograft were placed into individual wells of a 24-well plate in triplicate and repeated three times. Cross-contamination of allografts between the wells was prevented by leaving an empty well between the samples. Human bone marrow–derived mesenchymal stem cells (hBMSCs; $1.5 \times 10^{5;}$ ATCC) in 300 µL of MSC growth medium (ATCC) were seeded on the allografts and incubated at 37°C for 4 hours. Following the 4-hour incubation period, another 700 µL of MSC growth medium were added to the wells, and the culture continued for another 20 hours. Samples were collected for cell adhesion measurements after 1 day. For the 3- and 7-day cultures, allografts with the adherent cells were transferred to fresh wells, and the culture continued. The cell culture medium was refreshed every 2 to 3 days. The number of adherent cells on the allografts was quantified using a cell-counting kit (CCK-8, Dojindo Molecular Technologies) according to the manufacturer's protocol. Briefly, after 1, 3, and 7 days, the MSC growth medium with a tetrazolium-monosodium salt solution was added to the samples and incubated at 37°C for 1 hour. A total of 100 µL of the incubated solution was then transferred to 96-well plates, and the absorbance was measured at 450 nm with a plate reader (Synergy Multimode Reader, Agilent).

In addition, the adherent and proliferated cells on the allografts at 7 days were visualized by staining them with a live/dead viability-cytotoxicity kit (Thermo Fisher Scientific). The samples were incubated with live/dead assay reagents at room temperature for 30 minutes, and the stained cells were observed through a fluorescent microscope (BX53, Olympus).

Scanning electron microscopy of adherent cells. The morphology of adherent cells on the allografts was characterized via SEM. Following the 7-day incubation period, the grafts with the adherent cells were fixed in 2% and 4% paraformaldehyde for 10 and 20 minutes, respectively. The fixed cells were then dehydrated using a graded series of ethanol (50%, 75%, 95%, and 100% diluted in DI-H_2O) followed by a graded series of hexamethyldisilazane (HMDS; 25%, 50%, 75%, and 100% diluted in ethanol) for 15 minutes. Dehydrated samples were left in 100% HMDS overnight until they were completely dry, then images were taken using an SEM (JSM 6460LV, JEOL).

Alkaline phosphatase activity. The hBMSCs were cultured for 21 days in triplicate using the same protocol described above. After 21 days of incubation, the adherent cells on the allografts were trypsinized and collected. The alkaline phosphatase (ALP) activity was quantified with an alkaline phosphatase assay kit

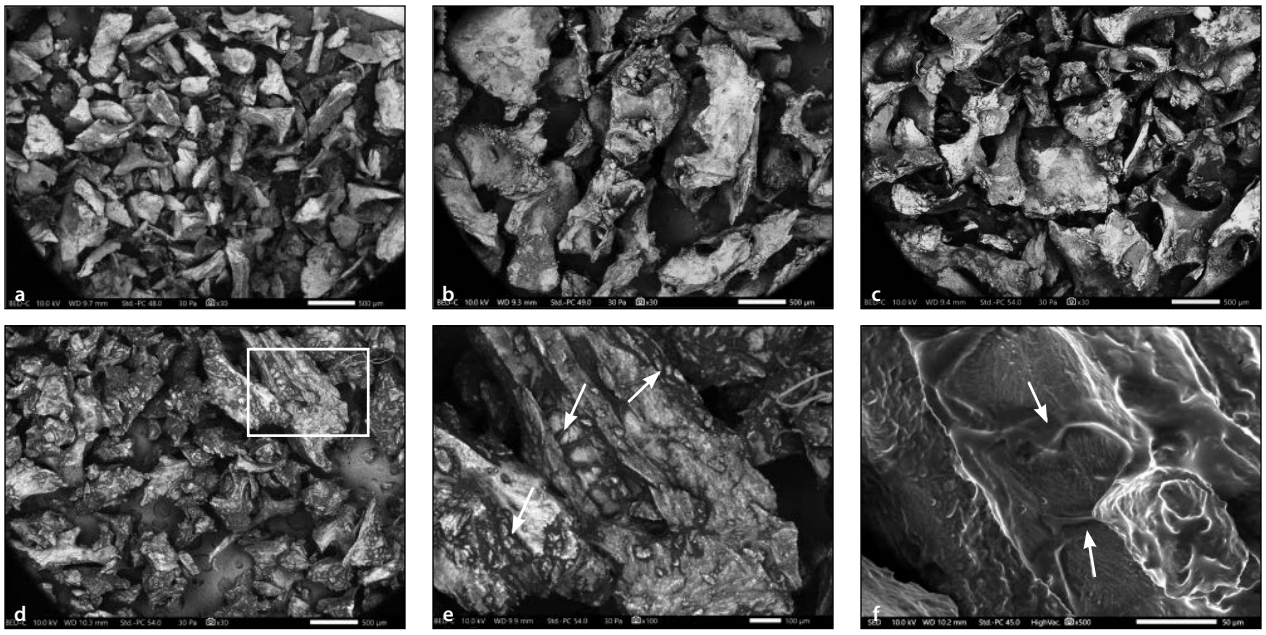

Fig 1 Low-magnification SEM micrographs of *(a)* PTA, *(b)* CFA, *(c)* OFA, and *(d)* MFA, showing the size and shape of the particulates (scale bars = 500 µm). The three freeze-dried samples have a larger particle size range compared to PTA. *(d)* MFA exhibits some surface features seen in the boxed area as the darker network structure, and at higher magnifications, ie, *(e)* scale bar = 100 µm and *(f)* scale bar = 50 µm. The white arrows in *(e)* point to these features that are distinguishable from the underlying lighter gray mineralized particulate matter. The arrows in *(f)* show the network structure in more detail, which has stretched and opened between the underlying collagen fiber bundles.

(BioVision) following the manufacturer's protocol. The total protein was measured by a pierce rapid gold BCA protein assay kit (Thermo Fisher Scientific) and used to normalize the data.

Statistical Analysis

All experiments were performed in biologic replicates ($n \geq 3$). The data are shown as means with standard deviation. One-way ANOVA with Tukey post hoc test was performed with GraphPad Prism 8.0. The Pearson correlation coefficient was calculated to identify the relationships between element contents and hardness value. *P* values < .05 were considered significant.

RESULTS

Physical and Chemical Characterization of the Allografts

The representative low-magnification back-scattered electron images, as shown in Fig 1a to 1d, revealed differences in the overall architecture of the bone particulates. Although the nominal size ranges for PTA, CFA, and OFA were given by the suppliers as 0.25 to 1 mm and MFA was given as 0.3 to 1 mm, the size distribution was evidently smaller in PTA compared to the three other allografts. Even at such low magnification, some differentiating surface features were obvious, such as the darker network features seen on MFA, which are visible within the boxed area in Fig 1d and illustrated at higher magnifications in Figs 1e and 1f. These structures, which contrast starkly with the lighter underlying mineralized particulate matter, were unidentifiable, suggesting an organic composition and a form not recognizable as normal bone structure.

Fig 2 shows three sets of higher-magnification views of all four allografts: PTA, CFA, OFA, and MFA. Though all samples appeared very similar at the lowest magnification (Figs 2a, 2d, 2g, and 2j; scale bars = 10 µm), with obvious collagen bundle directionality in the bone structure, the collagen fiber structure was less distinct on the three freeze-dried allografts compared to that of PTA at higher magnifications (Figs 2b, 2e, 2h, and 2k; scale bars = 5 µm). In addition, the collagen fibers appeared to be covered by a thin organic film in the OFA sample. These differences were most obvious at the highest magnification series (Figs 2c and 2l; scale bars = 1 µm), where PTA (Fig 2c) had clearly visible fine collagen fibrils running obliquely to the underlying collagen fiber bundles, while the film in OFA (Fig 2i) was evident through the defects that had opened between the underlying collagen fiber bundles. By comparison, the collagen structure in both CFA and MFA became less distinct, with no evident fine structure at this magnification. Indeed, by further increasing the magnification, as shown in Figs 2m and 2n, the collagen fibers of the PTA surface exhibited a distinct crossbanding motif in the 45- to 71-nm scale range, while the MFA surface also possessed a surface film that appeared buckled. Although these appearances may be considered to be

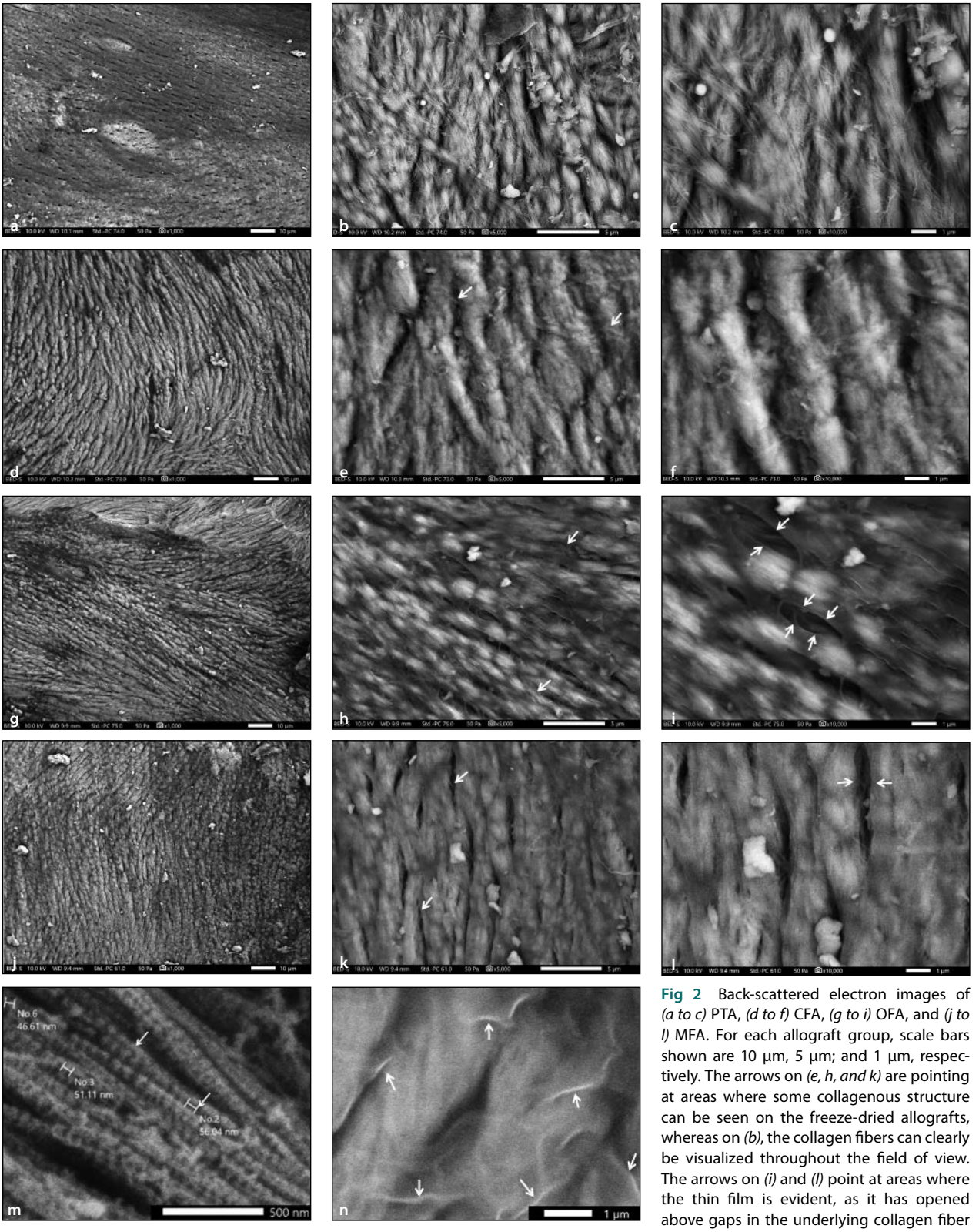

Fig 2 Back-scattered electron images of *(a to c)* PTA, *(d to f)* CFA, *(g to i)* OFA, and *(j to l)* MFA. For each allograft group, scale bars shown are 10 µm, 5 µm; and 1 µm, respectively. The arrows on *(e, h, and k)* are pointing at areas where some collagenous structure can be seen on the freeze-dried allografts, whereas on *(b)*, the collagen fibers can clearly be visualized throughout the field of view. The arrows on *(i)* and *(l)* point at areas where the thin film is evident, as it has opened above gaps in the underlying collagen fiber structure. *(m)* A higher magnification of the collagen fiber structure of PTA shows a crossbanding structure (arrows; not seen on the other allografts). Scale bar = 500 nm. *(n)* The buckled film (arrows) on the MFA sample Scale bar = 1 µm).

artifacts of sample preparatory processing, the crossbanding nevertheless approximates the known 64-nm crossbanding seen in collagen fibers, while the buckled film on MFA may be similar to that evident on the OFA sample.

The above comparisons clearly demonstrate that the PTA samples exhibited the least modified fine-surface structure when compared to the

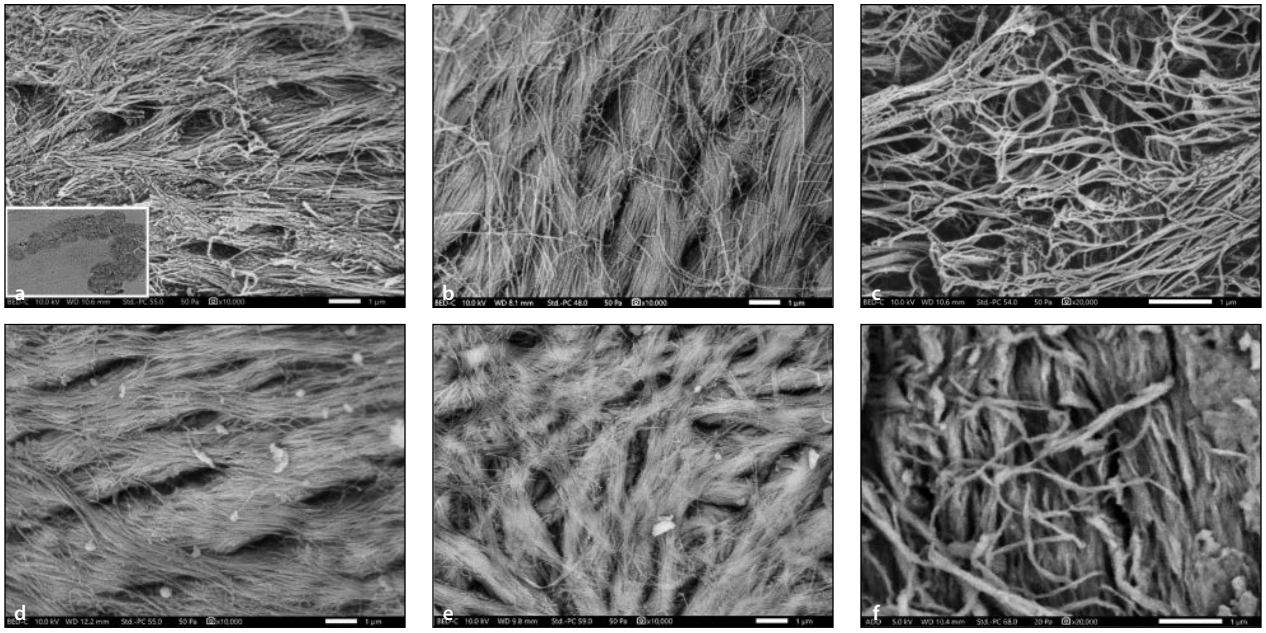

Fig 3 Back-scattered electron images of *(a to c)* human bone and *(d to f)* PTA (scale bar = 1 μm). The bundles of collagen and individual collagen fibrils are very similar in both. At higher magnification, the collagen fibrils on both *(c)* human bone and *(f)* PTA (scale bar = 1 μm) can be seen. Note: The inset image in *(a)* shows the type of resorption track left by osteoclasts in vitro from which the images in *(a)* and *(b)* are taken (field width: 81 μm).

other allografts. The comparison between this and a natural bone surface prepared by the resorptive activity of osteoclasts is illustrated in Fig 3, where Figs 3a to 3c are images from an in vitro–generated osteoclast resorption track in human bone, as shown in the inset in Fig 3a, while Figs 3d to 3f are images at the equivalent magnifications from a PTA surface. The comparison of Figs 3a, 3b, 3d, and 3e, which are all the same magnification, illustrates the close similarity between both the collagen fiber bundle and collagen fibril arrangements on both substrates. Indeed, at higher magnifications (Figs 3c and 3f), PTA processing has clearly maintained the fine bone structure, including the crossbanding of the collagen fibers (arrow in Fig 3f).

Surface roughness analysis of the allografts and human bone sample also confirmed the qualitative observations made by SEM imaging. PTA (8.34 μm) showed the closest Sa value to that of human bone (9.91 μm), followed by CFA (7.22 μm), OFA (6.55 μm), and MFA (5.36 μm). It should be emphasized that the software converts the luminance information to topography to measure these Sa values, and given the challenges that faced the freeze-dried allograft imaging due to extensive electron charging, the brightness, contrast, and probe current had to be adjusted in order to capture somewhat clear images. This may partially impact the measurements, and therefore the reported Sa values should not be treated as absolute values, but rather used as a comparative semiquantitative analysis to confirm the observations made by SEM imaging.

BET analysis exhibited a specific surface area for PTA that was two orders of magnitude higher than the other allografts (Fig 4a). There were no significant differences in the surface areas of CFA, OFA, and MFA (Fig 4a).

As seen from the XRD patterns in Fig 4b, the only phase identified for all the tested allografts is crystalline hydroxyapatite, without any noticeable presence of tricalcium phosphates (α-TCP or β-TCP) or CaO phases. A typical crystallite size of approximately 7 nm was measured for all allografts, without any significant differences between the allografts (Table 2).

The hardness values shown in Fig 4c exhibited a significantly higher ($P < .001$) value for CFA (> 40 HV), which was within the range reported in the literature for human bone (ie, ~ 32 to 45 HV) compared to other allografts (< 30 HV). When the amounts of calcium and phosphorous were measured by ICP, significantly higher calcium and phosphorus content was also seen for CFA compared to other allografts (Figs 4d and 4e), however, they both were above the calcium and phosphorus weight percentage range reported for human bone (as shown by dashed lines). The calcium phosphate ratios were, however, comparable between all allografts (Fig 4f), as was the nitrogen content (Fig 4g), which measured significantly lower than the range reported for human bone (as shown by dashed lines).

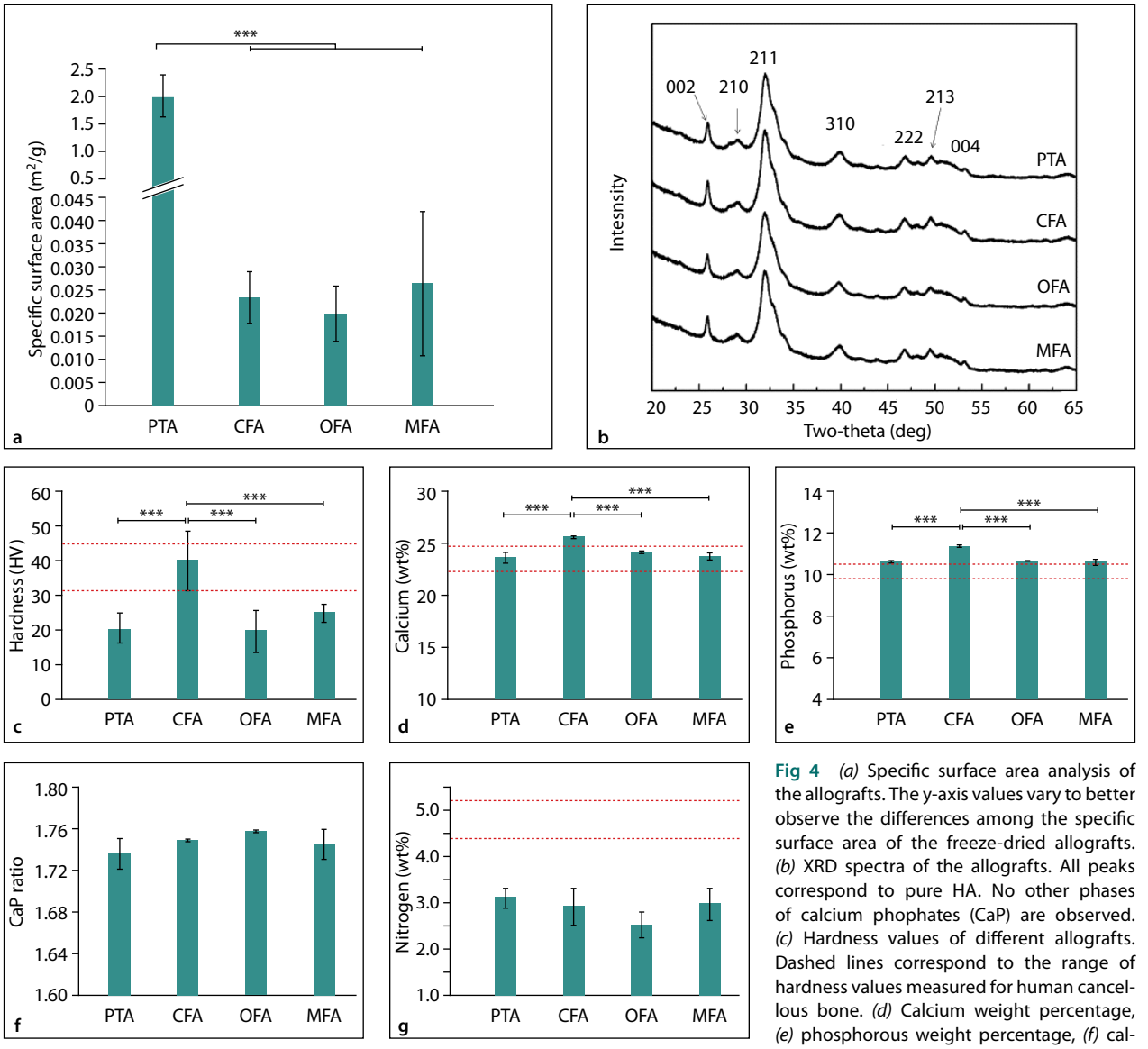

Fig 4 *(a)* Specific surface area analysis of the allografts. The y-axis values vary to better observe the differences among the specific surface area of the freeze-dried allografts. *(b)* XRD spectra of the allografts. All peaks correspond to pure HA. No other phases of calcium phophates (CaP) are observed. *(c)* Hardness values of different allografts. Dashed lines correspond to the range of hardness values measured for human cancellous bone. *(d)* Calcium weight percentage, *(e)* phosphorous weight percentage, *(f)* calcium to phosphorous ratio, and *(g)* nitrogen weight percentage of the allografts measured by ICP-AES. Dashed lines correspond to the estimated range obtained from literature for human cancellous bone. Adjusted *P* values are shown in the tables.

	Adjusted *P* value				
	HV	**Ca wt%**	***P* wt%**	**CaP ratio**	**N wt%**
CFA vs PTA	< .001***	< .001***	< .001***	.5755	.8864
OFA vs PTA	.9899	.2766	.8056	.1485	.2139
MFA vs PTA	.5123	.8888	.9936	.7516	.9668
OFA vs CFA	< .001***	< .001***	< .001***	.6960	.5114
MFA vs CFA	< .001***	< .001***	< .001***	.9881	.9929
MFA vs OFA	.35	.9152	.9152	.52	.3806

***$P < .001$.

Table 2 Crystallite Sizes of Different Allografts as Calculated by Scherrer Equation Using the XRD Spectra

Crystallite size (nm, mean ± SD)	PTA	CFA	OFA	MFA
Overall	6.9 ± 0.6	8.1 ± 0.3	7.8 ± 0.3	8.1 ± 0.6
C-axial	24.8 ± 0.5	25.7 ± 0.7	25.3 ± 1.4	26.2 ± 0.7

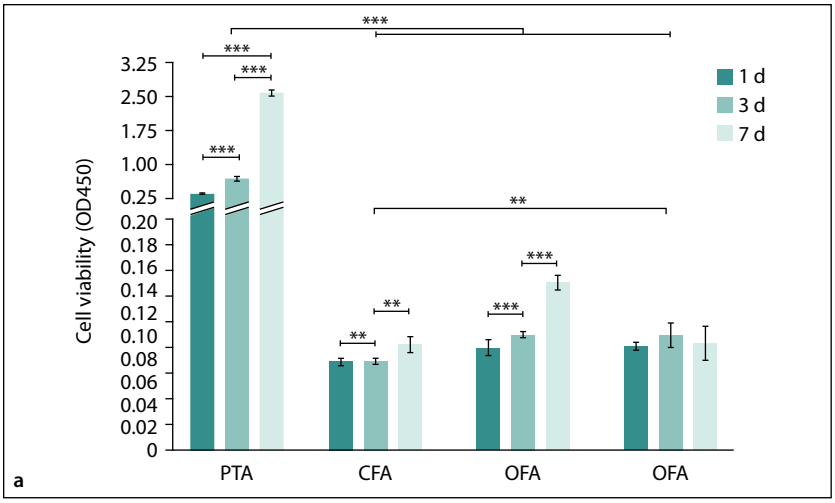

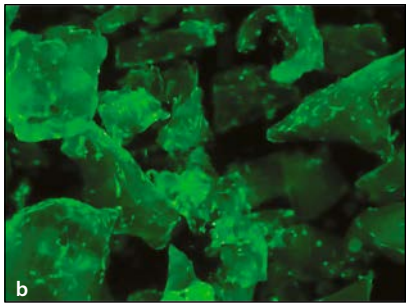

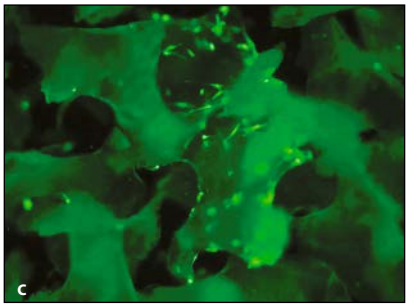

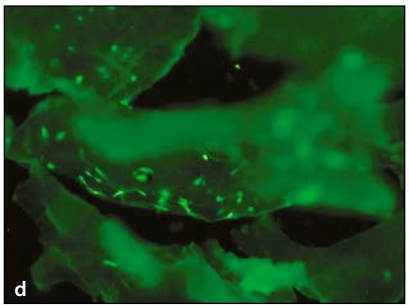

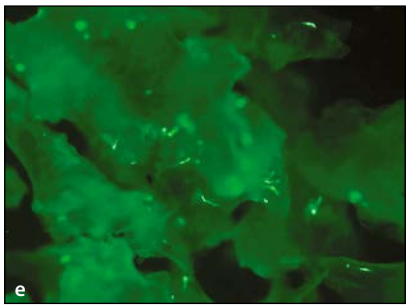

Fig 5 *(a)* Cell viability on different allografts at 1, 3, and 7 days. The y-axis values vary to better observe the differences among the freeze-dried allografts. *(b to e)* Fluorescent images of PTA, CFA, OFA, and MFA following live/dead staining at 7 days, respectively. Different planes and depth of field were examined with the freeze-dried allografts. However, only a few isolated cells could be visualized on the particulates on some planes. Indeed, the images included here for the freeze-dried allografts are from a plane with maximum number of cells. On the other hand, the PTA allograft showed cells on all the particulates on all the planes and depth of field examined similar to that shown in *(b)*. Adjusted *P* values are shown in the tables for different comparisons. Note: Very few dead cells were visualized on any of the allografts. They might have detached during the washing process in preparation for microscopy.

	Adjusted *P* value			
	1 d	**3 d**	**7 d**	
CFA vs PTA	< .001***	< .001***	< .001***	
OFA vs PTA	< .001***	< .001***	< .001***	
MFA vs PTA	< .001***	< .001***	< .001***	
OFA vs CFA	.8793	.437	.0029**	
MFA vs CFA	.8322	.4571	.9988	
MFA vs OFA	.9996	> .999	.0045**	
	PTA	**CFA**	**OFA**	**MFA**
3 d vs 1 d	< .001***	.9968	.0661	.4784
7 d vs 1 d	< .001***	.0083**	< .001***	.9244
7 d vs 3 d	< .001***	.0066**	< .001***	.6961

**P < .01, ***P < .001.

Cell Adhesion on the Allografts

A significantly higher (P < .001) number of hBMSCs were seen on PTA allograft compared to the freeze-dried allografts at all time points (Fig 5a). As indicated by the results in Fig 5a, only PTA significantly enhanced (P < .001) the number of adherent cells at the initial stage from 1 to 3 days. At 3 to 7 days, the cell number was significantly increased (P < .001 for PTA and OFA, and P = .0066 for CFA) on all allografts except for MFA (Fig 5a). At 7 days, PTA showed the highest number of viable cells (P < .001) compared to all freeze-dried allografts. Through live/dead staining, more cells were visualized on PTA than the freeze-dried allografts, regardless of the depth of the field (Figs 5b to 5e). Furthermore, the morphology of the adherent cells on the allografts showed marked differences (Figs 6a to 6d). Cells on PTA appeared more spread, and in some cases polygonal, with more cell processes (both pseudopods and filopodia), thereby providing greater numbers of substrate contact points compared to the needle-shaped cells on the freeze-dried allografts.

The ALP activity of the MSCs cultured on PTA was significantly higher (P < .001) than all other allografts after 21 days (Fig 6e). Among the freeze-dried allografts, cells cultured on CFA showed significantly less ALP activity than OFA (P = .0411). OFA showed higher ALP activity compared to MFA; however, the difference was not statistically significant (Fig 6f).

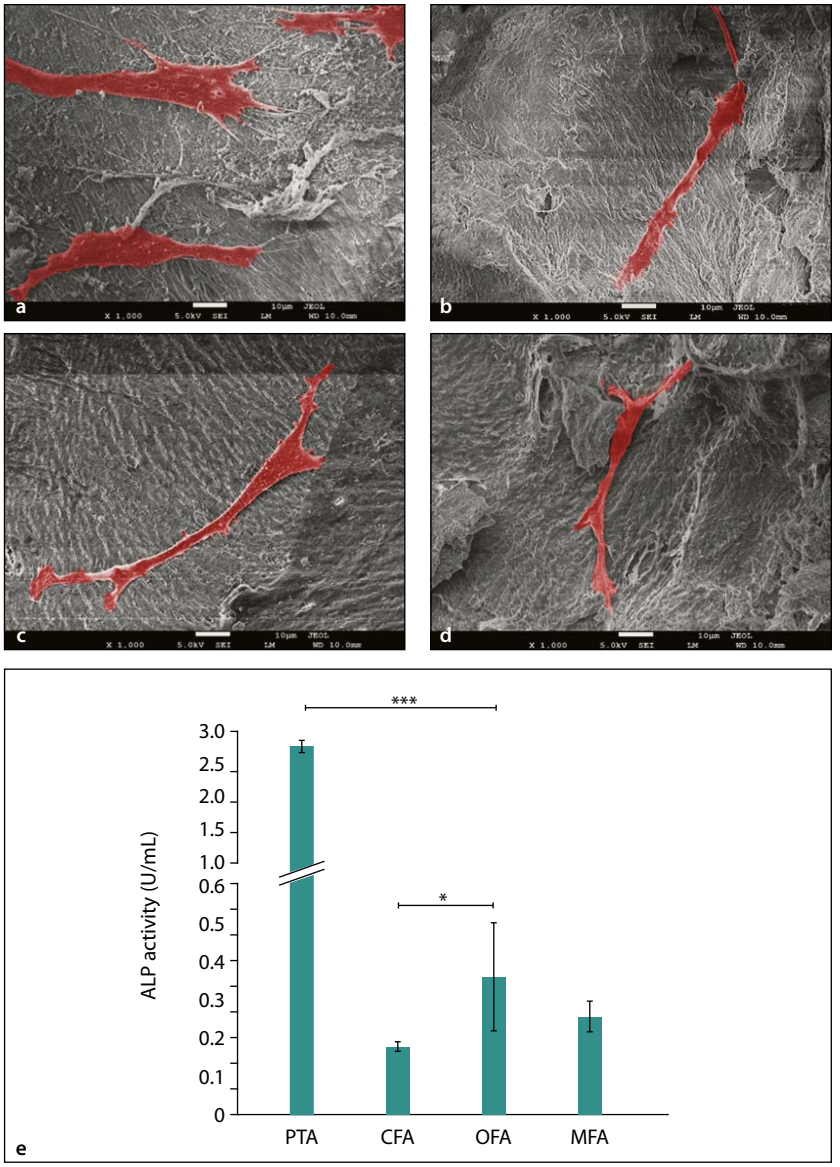

Fig 6 SEM micrographs of cells adhered to the allografts. *(a)* Cells on PTA are stretched and exhibit both pseudopods and filopodia. Note cells in upper right corner are polygonal in shape. *(b to d)* Cells on CFA, OFA, and MFA, respectively, are more needle-shaped with less evidence of filopodia. Note: Cells have been color coded in red using Adobe Photoshop for ease of visualization. *(e)* ALP activity of the hBMSCs cultured on the allografts at 21 days. The y-axis values vary to better observe the differences among the freeze-dried allografts. Adjusted *P* values are shown in the table.

	Adjusted *P* value
CFA vs PTA	< .001***
OFA vs PTA	< .001***
MFA vs PTA	< .001***
OFA vs CFA	.0411*
MFA vs CFA	.5727
MFA vs OFA	.3334

*$P < .05$, ***$P < .001$.

DISCUSSION

The findings herein clearly show that different processing methods result in different allograft physicochemical properties.

The most striking differences between allografts were seen with measurement of specific surface area and the morphology of the collagen microstructure. Specifically, the surface area of PTA was two orders of magnitude higher than that of the freeze-dried allografts, and the collagen microstructure—and the size of individual fibers—was almost identical to those seen with the osteoclast-resorbed human bone surface. The crossbanding of collagen fibers observed with PTA was further confirmation of minimally altered collagen structure.

Indeed, both the surface area and surface texture of a bone substitute influence cell attachment, proliferation, and differentiation,[19] which was observed in the culture of MSCs on the surfaces of the four allografts studied. More viable cells were enumerated and qualitatively visualized by fluorescence microscopy on PTA at all time points, which has a higher surface area compared to the freeze-dried allografts (Fig 4a). The polygonal cell morphology observed on PTA may also indicate a more favorable microenvironment compared to the thinner and more stretched cells found on the freeze-dried allografts. Indeed, it has been shown that increased specific surface area can offer more protein adsorption sites, facilitate the interactions between scaffolds and cells,[20] and lead to faster resorption of the graft in vivo[21]—a finding that has recently been

modeled by theoretical consideration of structural geometry of the bone substitutes.[22] On the contrary, a reduction in the specific surface area reduces the ligand density available to which cells could bind.[23] Indeed, Monje et al[24] compared PTA and MFA in maxillary sinus augmentation and observed that PTA had an accelerated turnover and fewer residual particles compared to MFA. They attributed this outcome to the solvent dehydration process and better collagen matrix preservation with PTA.

In addition, the ALP activity of MSCs cultured on PTA was significantly higher than other freeze-dried allografts (Fig 5), indicating its higher osteogenic potential. Among the freeze-dried allografts, the lowest ALP activity of MSCs was observed with CFA. It is known that the degradation of Ca^{2+}-containing biomaterials produces a localized calcium-rich osteoinductive microenvironment[25] and that extracellular calcium and other growth factors have a promigratory effect on MSCs.[26] Furthermore, even though CFA had the highest hardness and was the only allograft with a hardness value within the range reported for human appendicular bone (32.9 ± 6.6[27] to 43.82 HV[28], which is attributable to the significantly higher Ca content of CFA compared to MFA and OFA; Fig 4), the release of Ca should be less compared to the other allografts, thus reducing the impact on MSC differentiation. Indeed, there was a strong positive correlation between hardness values with calcium ($r = 0.937$, $P = .063$) and phosphorous ($r = 0.963$, $P = .037$) content. Nevertheless, calcium and phosphorous weight percentages and calcium phosphate ratios of the allografts, except CFA, were within the range determined by Akesson et al[29] for human trabecular bone.

It has been shown that the rate at which a calcium phosphate–based material is resorbed in vivo depends on several biomaterial-related factors, such as calcium and phosphorous content and their ratio, crystallinity, particle size, surface area, and porosity, along with factors related to the local biologic environment.[30] Moreover, it is known that for a given crystalline calcium phosphate, decreased crystal size results in accelerated dissolution.[31,32] No differences were detected either in the crystalline phase of the allografts on the XRD patterns or with the crystal size, all of which were within the range reported for human bone.[33,34] Therefore, it is reasonable to assume that the higher Ca content and hardness of CFA may lead to its slower resorption in vivo compared to the other allografts. In fact, this was shown in a clinical study that investigated healing of extraction sockets filled with CFA and PTA at 12 weeks and reported more residual graft particles and less vital bone on the sites treated with CFA compared to PTA.[35] By contrast, the nitrogen content of all examined allografts, which is a measure of the bone collagen matrix, was significantly below the range of 4.2% to 5.3% for natural human bone reported by Baker et al.[36]

Therefore, while there were general similarities in the chemical and physical characteristics of the studied allografts, significant differences were detected in calcium and phosphorous content, specific surface area, microarchitecture of the collagen compartment, and in vitro colonization behavior of MSCs. Although the results of these in vitro and ex vivo assays cannot be employed to predict the clinical performance of the grafts, the findings of the present study will facilitate an understanding of the impact of processing and sterilization methods on the physicochemical characteristics of the grafts and question the assumption that all bone allografts exhibit equivalent clinical performance. Further clinical studies are warranted to assess the impact of such differences on the clinical performance of such allograft materials.

CONCLUSIONS

Commercially available cancellous bone allografts differ in their specific surface area, calcium and phosphorous content, and bone particulate microarchitecture. These physicochemical differences result from different tissue processing and sterilization methods undertaken by the tissue banks, which differentially impact the response of MSCs in vitro and may alter their biologic performance in vivo.

ACKNOWLEDGMENTS

The authors are grateful to Dr Birol Ay for providing the human bone samples, which were part of a previously published study.[18] The authors also thank Professor J. E. Davies for his review of both the manuscript and the data presented. All authors were employees of Zimmer Biomet during the conduction of this study.

REFERENCES

1. Sargozaie N, Moeintaghavi A, Shojaie H. Comparing the quality of life of patients requesting dental implants before and after implant. Open Dent J 2017;11:485–491.
2. Sakkas A, Wilde F, Heufelder M, Winter K, Schramm A. Autogenous bone grafts in oral implantology-is it still a "gold standard"? A consecutive review of 279 patients with 456 clinical procedures. Int J Implant Dent 2017;3:23.
3. Stevenson S, Emery SE, Goldberg VM. Factors affecting bone graft incorporation. Clin Orthop Relat Res 1996;324:66–74.
4. Wang W, Yeung KWK. Bone grafts and biomaterials substitutes for bone defect repair: A review. Bioact Mater 2017;2:224–247.
5. Khan SN, Cammisa FP Jr, Sandhu HS, Diwan AD, Girardi FP, Lane JM. The biology of bone grafting. J Am Acad Orthop Surg 2005;13:77–86.
6. Deijkers RL, Bouma GJ, van der Meer-Prins EM, Huysmans PE, Taminiau AH, Claas FH. Human bone allografts can induce T cells with high affinity for donor antigens. J Bone Joint Surg Br 1999;81:538–544.

7. Rasch A, Naujokat H, Wang F, Seekamp A, Fuchs S, Klüter T. Evaluation of bone allograft processing methods: Impact on decellularization efficacy, biocompatibility and mesenchymal stem cell functionality. PLoS One 2019;14:e0218404.
8. Vangsness Junior CT. Allografts: Graft sterilization and tissue banking safety issues graft sterilization and tissue banking safety issues. In: Noyes FR (ed). Noyes' Knee Disorders: Surgery, Rehabilitation, Clinical Outcomes, ed 1. Philadelphia: Saunders Elsevier, 2010:240–244.
9. Moon KN, Kim SG, Oh JS, Kim CS, Lim SC, Jeong MA. Evaluation of bone formation after grafting with deproteinized bovine bone and mineralized allogenic bone. Implant Dent 2015;24:101–105.
10. Singh R, Singh D, Singh A. Radiation sterilization of tissue allografts: A review. World J Radiol 2016;8:355–369.
11. Park JY, Gemmell CH, Davies JE. Platelet interactions with titanium: Modulation of platelet activity by surface topography. Biomaterials 2001;22:2671–2682.
12. Oprea WE, Karp JM, Hosseini MM, Davies JE. Effect of platelet releasate on bone cell migration and recruitment in vitro. J Craniofac Surg 2003;14:292–300.
13. Barberi A, Samarani A, Nader N, et al. Physicochemical characteristics of bone substitutes used in oral surgery in comparison to autogenous bone. Biomed Res Int 2014;2014:320790.
14. Anil A, Sadasivan A, Koshi E. Physicochemical characterization of five different bone graft substitutes used in periodontal regeneration: An in vitro study. J Int Soc Prev Community Dent 2020;10:634–642.
15. Tadic D, Epple M. A thorough physicochemical characterization of 14 calcium phosphate-based bone substitution materials in comparison to natural bone. Biomaterials 2004;25:987–994.
16. Mauro CS, Rihn JA, Harner CD. Chapter 12 - Safety issues for musculoskeletal allografts: The stiff knee. In: Johnson DL, Mair SD, (Eds). Clinical Sports Medicine. Philadelhpia: Mosby, 2006:111–116.
17. Vaishnav S, Thomas Vangsness C Jr, Dellamaggiora R. New techniques in allograft tissue processing. Clin Sports Med 2009;28:127–141.
18. Ay B, Mendes VC, Zhang L, Davies JE. A "best fit" approach for synergistic surface parameters to guide the design of candidate implant surfaces. J Biomed Mater Res B Appl Biomater 2019;107:2165–2177.
19. Hing KA. Bioceramic bone graft substitutes: Influence of porosity and chemistry. Int J Appl Ceram Technol 2005;2:184–199.
20. Zhang K, Fan Y, Dunne N, Li X. Effect of microporosity on scaffolds for bone tissue engineering. Regen Biomater 2018;5:115–124.
21. Eggli PS, Müller W, Schenk RK. Porous hydroxyapatite and tricalcium phosphate cylinders with two different pore size ranges implanted in the cancellous bone of rabbits. A comparative histomorphometric and histologic study of bony ingrowth and implant substitution. Clin Orthop Relat Res 1988;232:127–138.
22. Bohner M, Baumgart F. Theoretical model to determine the effects of geometrical factors on the resorption of calcium phosphate bone substitutes. Biomaterials 2004;25:3569–3582.
23. Murphy CM, O'Brien FJ. Understanding the effect of mean pore size on cell activity in collagen-glycosaminoglycan scaffolds. Cell Adh Migr 2010;4:377–381.
24. Monje A, O'Valle F, Monje-Gil F, et al. Cellular, vascular, and histomorphometric outcomes ofsolvent-dehydrated vs freeze-dried allogeneic graft for maxillary sinus augmentation: A randomized case series. Int J Oral Maxillofac Implants 2017;32:121–127.
25. Aquino-Martínez R, Angelo AP, Pujol FV. Calcium-containing scaffolds induce bone regeneration by regulating mesenchymal stem cell differentiation and migration. Stem Cell Res Ther 2017;8:265.
26. González-Vázquez A, Planell JA, Engel E. Extracellular calcium and CaSR drive osteoinduction in mesenchymal stromal cells. Acta Biomate 2014;10:2824–2833.
27. Dall'Ara E, Ohman C, Baleani M, Viceconti M. The effect of tissue condition and applied load on Vickers hardness of human trabecular bone. J Biomech 2007;40:3267–3270.
28. Wu WW, Zhu YB, Chen W, et al. Bone hardness of different anatomical regions of human radius and its impact on the pullout strength of screws. Orthop Surg 2019;11:270–276.
29. Akesson K, Grynpas MD, Hancock RG, Odselius R, Obrant KJ. Energy-dispersive X-ray microanalysis of the bone mineral content in human trabecular bone: A comparison with ICPES and neutron activation analysis. Calcif Tissue Int 1994;55:236–239.
30. Hannink G, Arts JJ. Bioresorbability, porosity and mechanical strength of bone substitutes: What is optimal for bone regeneration? Injury 2011;42(suppl 2):s22–s25.
31. Barrère F, Stigter M, van Blitterswijk CA, Layrolle P, De Groot K. In vitro dissolution of various calcium-phosphate coatings on Ti6Al4V. Key Eng Mater 2001;192–195:67–70.
32. Barrère F, van Blitterswijk CA, de Groot K. Bone regeneration: Molecular and cellular interactions with calcium phosphate ceramics. Int J Nanomedicine 2006;1:317–332.
33. Handschin RG, Stern WB. X-ray diffraction studies on the lattice perfection of human bone apatite (Crista Iliaca). Bone 1995;16(suppl):s355–s363.
34. Jackson SA, Cartwright AG, Lewis D. The morphology of bone mineral crystals. Calcif Tissue Res 1978;25:217–222.
35. Lipton DI. Clinical and Histological Evaluation of Zimmer Puros Allografts vs. Creos Allograft for Alveolar Ridge Preservation Following Exodontia [thesis]. Gainesville: University of Florida, 2016.
36. Baker SL, Butterworth EC, Langley FA. The calcium and nitrogen content of human bone tissue cleaned by micro-dissection. Biochem J 1946;40:391–396.